

Total Denoising: Unsupervised Learning of 3D Point Cloud Cleaning

Pedro Hermosilla
Ulm University

Tobias Ritschel
University College London

Timo Ropinski
Ulm University

Abstract

We show that denoising of 3D point clouds can be learned unsupervised, directly from noisy 3D point cloud data only. This is achieved by extending recent ideas from learning of unsupervised image denoisers to unstructured 3D point clouds. Unsupervised image denoisers operate under the assumption that a noisy pixel observation is a random realization of a distribution around a clean pixel value, which allows appropriate learning on this distribution to eventually converge to the correct value. Regrettably, this assumption is not valid for unstructured points: 3D point clouds are subject to total noise, i. e., deviations in all coordinates, with no reliable pixel grid. Thus, an observation can be the realization of an entire manifold of clean 3D points, which makes a naïve extension of unsupervised image denoisers to 3D point clouds impractical. Overcoming this, we introduce a spatial prior term, that steers converges to the unique closest out of the many possible modes on a manifold. Our results demonstrate unsupervised denoising performance similar to that of supervised learning with clean data when given enough training examples - whereby we do not need any pairs of noisy and clean training data.

1. Introduction

While the amount of clean 3D geometry is limited by the manual effort of human 3D CAD modelling, the amount of 3D point clouds is growing rapidly everyday: our city's streets, the interior of everyday buildings, and even the goods we consume are routinely 3D-scanned. Regrettably, these data are corrupted by scanner noise and as such not accessible to supervised learning that requires pairs of noisy and clean data. Consequently, it is desirable to be able to denoise the thus acquired noisy 3D point clouds by solely using the noisy data itself.

Two necessary recent developments indicate that this might be possible: deep learning on 3D point clouds [20] and unsupervised denoising of images [18, 16, 3].

Unfortunately, these two methods cannot be combined naïvely. To learn our unsupervised 3D point cloud denoisers (Fig. 1), we need to overcome two main limitations: the

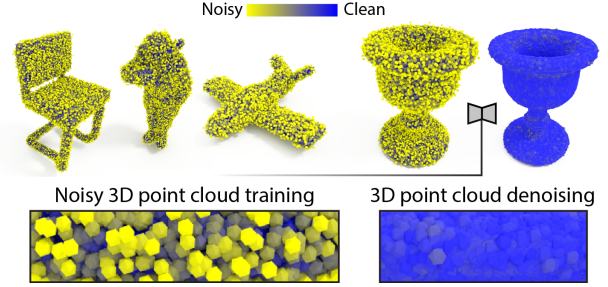


Figure 1. We learn 3D point cloud cleaning (right), unsupervised, from noisy examples alone (left).

practical obstacle to have a pair of two noisy scans of the same object and the theoretical difficulty that noise in 3D point clouds is *total*.

We refer to noise as ‘total’ (Fig. 2) when distortions are not confined to the range (pixel values) while the domain is clean (as pixel positions are), but to the more challenging setting where both domain and range are affected by noise. The name is chosen in analogy to total least squares [10], which dealt with simultaneous noise in domain and range, but for a linear, non-deep setting.

This paper’s evaluation shows for simulated noise of different kind, as well as for real point clouds, how our unsupervised approach nonetheless outperforms a supervised approach given enough, and in some cases even when given the same magnitude of, training data, while it runs efficiently in a single pass on large point clouds.

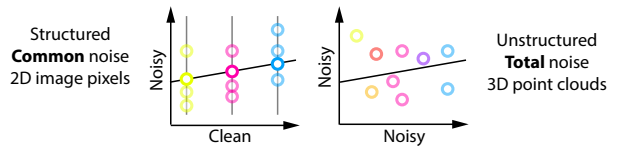


Figure 2. To learn denoising of 3D point clouds, we need to extend from common noise that is clean in one part of the signal, to a total setting, where all parts of the signal are noisy. This example shows three realizations of common noise (left) and total noise (right) for three samples (colors). Please note, how total noise is “more noisy” as both axis are corrupted.

2. Related Work

Image denoising. Denoising images is one of the most basic image manipulation operations. The most primitive variants are based on linear filters such as the Gaussian filter, eventually with additional sharpening [14]. While non-linear filters, such as median, bilateral [25] or non-local means [4] are frequently used in practice, state-of-the-art results are achieved by optimizing for sparsity [7]. Recently, it has become popular to learn denoising, when pairs of clean and noisy images are available [5].

Lehtinen et al. [18] proposed a method to learn denoising with access to only two noisy images, instead of a clean-noisy pair. Taking it a step further, Noise2Void [16] and Noise2Self [3] are two extensions that remove the requirement to have two copies of one image corrupted with noise and instead work on a single image. In both cases, this is achieved by regressing the image from itself. This is done by creating a receptive field with a “blind spot”, and a network regresses the blind spot from its context. We will detail the theory behind those papers [18, 16, 3] in Sec. 3.

3D point cloud denoising. 3D point clouds capture fine spatial details but remain substantially more difficult to handle than images, due to their irregular structure [19]. It is even difficult to come up with a general definition of a point cloud. One common interpretation is the fixed point surface of an iterated function, fitted using moving least-squares, mapping space to space [1].

Similar as for images, linear filters can be applied to remove noise [17], but at the expense of feature details. As a remedy, image operators such as bilateral [9, 6], non-local means [22] or sparse coding [2] have been transferred to point clouds.

With the advent of PointNet [20], deep learning-based processing of point clouds has become tractable. Two notable deep methods to denoise 3D point clouds were suggested. The first is PointProNet, that denoises patches of points by projecting them to a learned local frame and using Convolutional Neural Networks (CNN) in a supervised setup to move the points back to the surface [23]. However, the accuracy of the method is determined by the accuracy of the local frame estimation, which results in artifacts in extreme sharp edges. The second approach has been published by Rakotosaona et al. [21] and uses the PCPNet architecture [12] (a variant of PointNet [20]) to map noisy point clouds to clean ones. Both approaches are supervised, as they require pairs of clean and noisy point clouds, which in practice are produced by adding noise to synthetic point clouds. Our approach does not require such pairs.

Noise and learning. Noise is an augmentation strategy used in denoising auto-encoders [26]. These are however

not aiming to denoise, but add noise to improve robustness. Also is their target not noisy, but noise is in the input or added to internal states.

3. Denoising Theory

Based on denoising in the regular domain, i. e., images, with or without supervision, we will establish a formalism that can later also be applied to derive our unstructured 3D case.

3.1. Regular Domains

Pixel noise. An observation \mathbf{y}_i at pixel i in a noise corrupted image is a sample of a noise distribution $\mathbf{y}_i \sim p(\mathbf{z}|\mathbf{x}_i)$ around the true value \mathbf{x}_i . This is shown in Fig. 3, a). The black curve is the true signal and pixels (dotted vertical lines) sample it at fixed positions i (black circles) according to a sampling distribution $p(\mathbf{z}|\mathbf{x}_i)$ (yellow curve) around the true value (pink circle).

Supervised. In classic supervised denoising, we know both a clean \mathbf{x}_i and a noisy value $\mathbf{y} \sim p(\mathbf{z}|\mathbf{x}_i)$ for pixel i and minimize

$$\arg \min_{\Theta} \mathbb{E}_{\mathbf{y} \sim p(\mathbf{z}|\mathbf{x}_i)} l(f_{\Theta}(\mathbf{y}), \mathbf{x}_i),$$

where f is a tunable function with parameters Θ , and l is a loss such as L_2 . Here and in the following, we omit the fact that the input to f comprises of many \mathbf{y} that form an entire image, or at least a patch. We also do not show an outer summation over all images (and later, point cloud) exemplars.

Unsupervised, paired. Learning a mapping from one noisy realization of an image to another noisy realization of the same image is achieved by Noise2Noise [18]. It has been shown, that learning

$$\arg \min_{\Theta} \mathbb{E}_{\mathbf{y}_1 \sim p(\mathbf{z}|\mathbf{x}_i)} \mathbb{E}_{\mathbf{y}_2 \sim p(\mathbf{z}|\mathbf{x}_i)} l(f_{\Theta}(\mathbf{y}_1), \mathbf{y}_2),$$

converges to the same value as if it had been learned using the mean / median / mode of the distribution $p(\mathbf{z}|\mathbf{x})$ when l is L_2 / L_1 / L_0 . In most cases, i. e., for mean-free noise, the mean / median / mode is also the clean value. We refer to this method as ‘paired’, as it needs two realizations of the signal, i. e., one image with two realizations of noise.

Unsupervised, unpaired. Learning a mapping from all noisy observations in one image, except one pixel, to this held-out pixel is achieved by Noise2Void [16] and Noise2Self [3]:

$$\arg \min_{\Theta} \mathbb{E}_{\mathbf{y} \sim p(\mathbf{z}|\mathbf{x}_i)} l(f_{\Theta}(\mathbf{y}), \mathbf{y}),$$

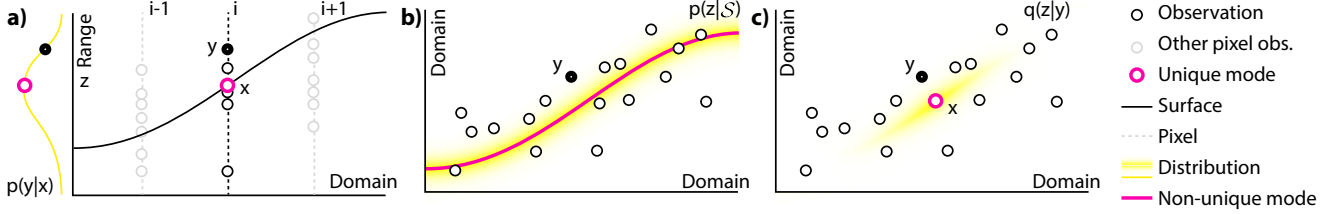


Figure 3. Substantial differences exist when denoising structured and unstructured data. (a) For structured data, each pixel value follows a sampling distribution $p(z|x_i)$ (yellow curve) around the true value (pink circle). (b) For unstructured data, the distribution $p(z|S)$ has a manifold of modes (pink line). (c) By using the proposed proximity-appearance prior, a unique mode closest to the surface is determined.

Here, f is a special form of \mathcal{J} -incomplete [3] maps that have no access to pixel i when regressing it, i.e., a ‘blind spot’. The same relation between mean / median / mode and loss as in Noise2Noise applies. Note that this formulation does not require two images, and we, therefore, refer to it as ‘unpaired’.

Discussion. All three methods described above, work under the assumption that, in a structured pixel grid, the range (vertical axis in Fig. 2, left and Fig. 3, a) axis i and the domain z (horizontal axis) have different semantics. The noise is only in the range: it is not uncertain *where* a pixel is, only what its true *value* would be.

3.2. Unstructured Domains

Point noise. As for pixels, we will denote clean points as x , noisy points as y and the noise model as p . All points in our derivation can be either positional with XYZ coordinates, or positional with appearance, represented as XYZRGB points.

To our knowledge, deep denoising of colored point clouds has not been proposed. We will not only show how our technique can also be applied to such data but moreover, how color can help substantially to overcome challenges when training unsupervised learning of a point cloud denoiser. Surprisingly, this benefit can be exploited during training, even when no color is present at test time. If available, it will help, and we can also denoise position and appearance jointly.

Supervised. Denoising a point cloud means to learn

$$\arg \min_{\Theta} \mathbb{E}_{y \sim p(z|S)} l(f_{\Theta}(y), S),$$

the sum of the losses l (e.g., Chamfer) between $f_{\Theta}(y)$ and the surface S of the 3D object. Such supervised methods have been proposed, but they remain limited by the amount of training data available [23, 21], as they require access to a clean point cloud.

4. Unsupervised 3D Point Cloud Denoising

We will first describe how a paired approach is not feasible for unstructured data before we introduce our unpaired, unsupervised approach.

4.1. Inapplicability of ‘paired’ Approaches

Learning a mapping $f_{\Theta}(\mathcal{Y}_1) = \mathcal{Y}_2$ from one noisy point cloud realization \mathcal{Y}_1 to another noisy point cloud realization \mathcal{Y}_2 that both have the same clean point cloud \mathcal{X} and where the i -th point in both point cloud is a realization of the i -th ground truth value, would be a denoiser in the sense of Noise2Noise [18]. Regrettably, Noise2Noise cannot be applied to unsupervised learning from unstructured point clouds for two reasons:

First, this paired design, same as for images, would require supervision in the form of two realizations of the same point cloud corrupted by different noise realizations. While this is already difficult to imagine for 2D image sensors, it is not feasible for 3D scanners. This is a practical reason.

Second, it would require a network architecture to know which point is which, similar as it is given by the regular structure of an image that explicitly encodes each pixel’s identity i . This is never the case for total noise in points. Opposed to this, modern convolutional deep point processing [20, 13] is exactly about becoming invariant under re-ordering of points. This reason is of theoretical nature.

In order to overcome this problem in a supervised setting, Rakotosaona et al. [21] simulated such pairing by selecting, for each noisy observation, the closest point in the clean point cloud as the target for the loss. However, this is only an approximation of the real surface whose accuracy depends on the quality of the sampling of the clean data. Fortunately, we can show that a pairing assumption is not required and our approach operates not only unsupervised but also unpaired as we will detail next.

4.2. Unpaired

Learning a mapping from a noisy realization to itself $f_{\Theta}(\mathcal{Y}) = \mathcal{Y}$ is an unsupervised and unpaired denoiser in the sense of Noise2Void [16] or Noise2Self [3]. Defining \mathcal{J} incompleteness in a point cloud is no difficulty: just prevent

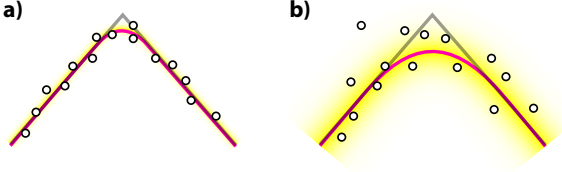


Figure 4. Comparing small (*left*) and large noise (*right*) we see the modes (*pink*) deviate from the GT surface (*black*).

access of f to point y itself when learning point y from the neighbors of y . Thus, essentially, we train a network to map each point to itself without information about itself. But there is the following catch with total noise.

Problem statement. Different from observing pixels at index i in an image (dotted line Fig. 3, a), which tell us that y is a realization of a hidden value x_i to infer, it is unknown which hidden surface point is realized when observing a point in an unpaired setting. A noisy point observation y , can be a realization of $p(z|x_1)$ in the same way as it could be a realization of $p(z|x_2)$. Consequently, the distribution $p(z|\mathcal{S})$ has a manifold of modes, depicted as a pink line in Fig. 3, b).

We, therefore, have to look into two questions: First, what can be said about the similarity of this manifold of modes and the clean surface? And second, how do we decide which of the many possible modes is the right one? Answering the second, and deriving bounds for the first question are the key contribution of this paper, enabling unsupervised 3D point cloud denoising.

4.3. Manifold of Modes vs. Clean Surface

Concerning the first question, the manifold of modes is close to the surface, but not identical. Fig. 4, a), shows a clean surface as a black line, with a small amount of noise, where most samples are close to the clean surface. In this condition, the learning converges to a solution identical to a solution it would have converged to when trained on the pink line, which is very similar to the clean surface. With more noise, however, it becomes visible in Fig. 4, b) that this manifold is not identical to the surface.

We note, that the mode surface is the convolution of the true surface and the noise model p . We cannot recover details removed by this convolution. This is different from supervised NN-based deconvolution, which has access to pairs of convolved and clean data. In our case, the convolution is on the limit case of the learning data and we never observe non-convolved, clean data.

It is worth noting, that not all noise distributions lead to a manifold that is a surface in 3D or would be a connected path in our 2D illustrations. Only uni-modal noise distribution, such a scanner noise, have no branching or dis-

connected components. Our solution will not depend on the topology of this mode structure.

4.4. Unique Modes

As explained above, the naïve implementation of unsupervised unpaired denoising will not have a unique mode to converge to. Therefore, we suggest regularizing the problem by imposing the prior $q(z|y)$ that captures the probability that a given observation y is a realization of the clean point z .

We suggest using a combination of spatial and appearance proximity

$$q(z|y) = p(z|\mathcal{S}) * k(z - y) \quad (1)$$

$$k(d) = \frac{1}{\sigma\sqrt{2\pi}} \exp\left(-\frac{\|Wd\|_2^2}{2\sigma^2}\right), \quad (2)$$

where σ is the bandwidth of k and $W = \text{diag}(w)$ is a diagonal weight matrix trading spatial and appearance locality. We use a value $w = 1/\alpha r$, r being 5% of the diameter of the model and α a scaling factor. In the case of point clouds with appearance, we use $w = \beta$ in the appearance rows/columns, otherwise, we only consider proximity. For more details about the values for such parameters please refer to the supplementary material.

This results in convergence to the nearest (in space and appearance) mode when optimizing

$$\arg \min_{\Theta} E_{y \sim p(z|\mathcal{S})} E_{q \sim q(z|y)} l(f_{\Theta}(y), q), \quad (3)$$

The effect of this prior is seen in Fig. 3, c). Out of the many modes of the distribution, the unique closest one remains.

Note, that our choice of Gaussian prior q is not related to a Gaussianity of the noise model p , which we do not assume. The only assumption made here is that out of many explanations, the closest one is correct.

Please also note, that the nearest mode is always defined, regardless of the topology of the mode structure, loops, branches etc. Our of any set of points, there is always a closest one.

Appearance to the rescue As mentioned above, 3D point clouds that come with RGB color annotation are a surprising opportunity to further overcome the limitations of unsupervised training. Otherwise, in some cases, the spatial prior cannot resolve round edges. This is not because the network f is unable to resolve them, but because unsupervised training does not ‘see’ the sharp details. Fig. 5 details how colors resolve this: without RGB, the corners are rounded in Fig. 5, a). When adding color, here red and blue (Fig. 5, b), the points become separated (Fig. 5, c). The sampling of the prior $q(z|y)$ on a red point, will never pick

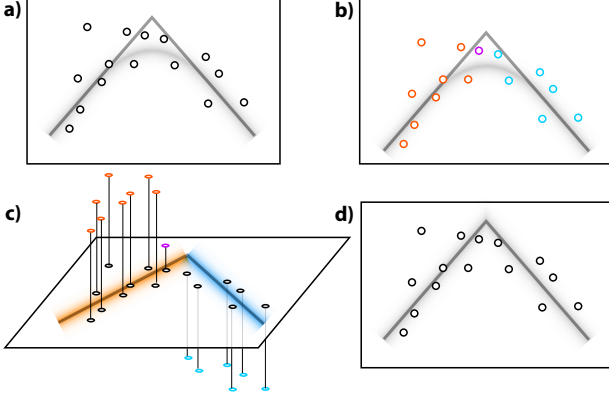


Figure 5. Bilaterality: The manifold of modes of the distribution of a 2D point cloud without color can be curved for strong noise (a). Different appearance, denoted as red and blue points in b, can be used to establish bilateral distances, lifting points to 3D. The resulting manifold of modes (d) now preserves sharp appearance edges.

a blue one and vice-versa. Consequently, the learning behaves as if it had seen the sharp detail.

Thus, in some way, using color in the prior reinforces some of the structure, which was lost when not relying on a regular pixel grid. We do not know which noisy point belongs to which measurement, but we have a strong indication, that something of different color, is not a noisy observation of the same point. Of course, it is possible, that two observations y_1 and y_2 appear to be from a different point, but happen to be measurements of the same clean surface point x , but having range noise affecting the color. Fortunately, such spurious false negatives are less problematic (they create variance) than the permanent false positives, that lead to rounding (bias).

Note, that the color was only required to sample the prior $q(z|y)$ and, therefore, to aid training to converge to a sharp mode. It is not suggested to use color as input to the network during testing. This might or might not be added on top.

4.5. Converging to the mode

We train the network to converge to the mode of the prior distribution $q(z|y)$ by using the approximation of the L_0 loss function proposed by Lehtinen et al. [18], $(|f_{\Theta}(y) - q| + \epsilon)^\gamma$, where their $\epsilon = 10^{-8}$, and their γ is annealed from 2 to 0 over the training.

Thus, our unsupervised training converges to the same as training supervised to find the closest – in XYZ space and RGB appearance, when available – mode on the distribution $S * p$ resulting from convolving the clean surface S and the noise model p .

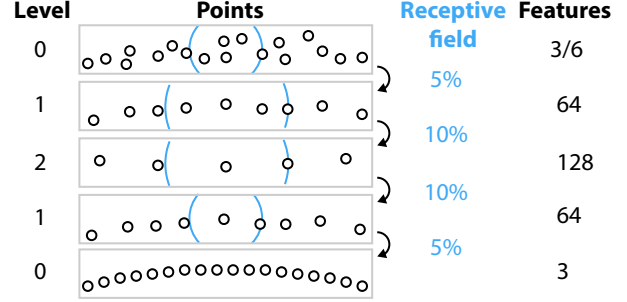


Figure 6. Architecture overview: We start from a noisy point cloud in the top and perform two levels of unstructured encoding, that reduce the receptive field, followed by two levels of decoding using transposed unstructured convolutions.

4.6. Implementation

Prior. To minimize Eq. 3 we need to draw samples according to the prior q which is implemented using rejection sampling: We pick a random point \hat{q} from \mathcal{Y} within r from y , and train on it only if $k(\hat{q} - y) > \xi$ for a uniform random $\xi \in (0, 1)$. In practice, a single sample is used to estimate this inner expected value over $q(z|y)$.

Architecture. We implement f using an unstructured encoder-decoder based on Monte Carlo convolution [13] (Fig. 6). Such an architecture consumes the point cloud, transforms spatial neighborhoods into latent codes defined on a coarser point (encoder) set, and up-sample these to the original point resolution (decoder). The effective receptive field, so the neighborhood from which the NN regressed points from themselves, is 30 % of the diameter of the model. In particular, we perform two levels of encoding, the first with a receptive field of 5 %, the second at 10 %. The Poisson disk radii for pooling in level one and two are half the size of the receptive fields.

This architecture is fast to execute, allowing to denoise in parallel 800 K points in 13 seconds in a single machine with a GeForce RTX 2080. Moreover, this architecture is composed of only 25 K trainable parameters, orders of magnitude smaller than other networks (0.8 million of PointNet or 1.4 million of PointNet++).

Training. While it could be demanding to appreciate why it can work, our method is simple to implement as seen in Alg. 1. Here, \mathcal{Q} denotes a set of prior samples q for all points in a point cloud. All operations are defined on batches that have the size of the point cloud. We use an ADAM optimizer [15] with an initial learning rate of .005, which is decreased during training.

Iteration. Similar as in previous work [21], we found results to improve if the output of the network is fed as input

Algorithm 1 Unsupervised point cloud denoiser training

```
1: for all noisy point clouds  $\mathcal{Y}$  do
2:    $\Xi \leftarrow \text{RANDOMUNIFORMBATCH}(0, 1)$ 
3:    $\mathcal{Q} \leftarrow \text{SAMPLEPRIORBATCH}(\mathcal{Y}, \Xi)$ 
4:    $\Theta \leftarrow \text{MINIMIZEBATCH}(\|f_{\Theta}(\mathcal{Y}) - \mathcal{Q}\|_0)$ 
5: end for
```

again. However, this introduces two problems: clustering of points, and shrinking of the point cloud after several iterations. We address these problems in a similar way as Rakotosaona et al. [21]. In order to prevent clustering we introduce the following regularization term that enforces an equidistant predicted point cloud:

$$L_r = \arg \min_{\Theta} \mathbb{E}_{\mathbf{y} \sim p(\mathbf{z}|\mathcal{S})} \max_{\mathbf{y}' \in n(\mathcal{Y}, \mathbf{y})} \|f_{\Theta}(\mathbf{y}), f_{\Theta}(\mathbf{y}')\|_2$$

where $n(\mathcal{Y}, \mathbf{y})$ is the set of points from the noisy point cloud within a patch centered at \mathbf{y} .

To prevent shrinking we remove the low-frequency displacements before translating the noisy points.

5. Evaluation

Our experiments explore the application, both to synthetic (Sec. 5.2) and to real data (Sec. 5.3). For synthetic data, we know the answer and can apply different metrics to quantify the performance of our approach, while we do not know the ground truth for real data and results are limited to a qualitative study.

5.1. Setup

Data set. We have collected 15 different classes with 7 different polygonal models each (5 for training and 2 for testing) from ModelNet-40 [29] and sampled the surface with points as explained next. As we optionally use RGB appearance, it is computed using Lambertian shading from 3 random directional lights.

Sampling. We simulate different forms of noise to corrupt the clean data of the synthetic data set.

In the SIMPLE noise model, we sample each 3D mesh using Poisson Disk sampling [27] to obtain clean point clouds within the range of 13 K and 190 K points each, resulting in 22 million points for training and 10 million points for testing. Then, we add Gaussian 3D noise with a standard deviation of .5%, 1%, and 1.5% of the diagonal of the bounding box to the coordinate.

The ADVANCED sampling emulates true sensor noise making use of Blendsor [11], a library to simulate sensor noise. In particular, we choose to emulate a Velodyne HDL-64E 3D scan. These devices introduce two types of noise in the measurements, a distance bias for each laser unit and

a per-ray Gaussian noise. In our data, we use a standard deviation of .5% of the diagonal of the bounding box for the distance bias and three different levels of per-ray noise, .5%, 1%, and 1.5%. This generates point clouds within the range of 3 K and 120 K points each, resulting in 12 million points for training and 5 million points for testing.

Metric. We use the Chamfer distance as proposed by Fan et al. [8],

$$d(\mathcal{Y}, \mathcal{S}, \mathcal{X}) = \frac{1}{N} \sum_{\mathbf{y} \in \mathcal{Y}} \min_{\mathbf{s} \in \mathcal{S}} \|\mathbf{y} - \mathbf{s}\|_2 + \frac{1}{M} \sum_{\mathbf{x} \in \mathcal{X}} \min_{\mathbf{y} \in \mathcal{Y}} \|\mathbf{y} - \mathbf{x}\|_2$$

where less is better. The first term measures the average distance between the predicted points to their closest point in a polygonal surface \mathcal{S} . The second term measures how the points are distributed in the ground truth surface.

Since the clean point clouds \mathcal{X} follow a Poisson Disk distribution, by measuring their distance to the closest predicted point we are able to determine if the surface is equally covered by our predictions.

The metric is applied in the test data with three different realizations of noise and averaged over two complete trainings to reduce variance in the estimate of the metric.

Methods. We compare our unsupervised approach with classical methods as well as supervised machine learning approaches. To obtain insights regarding the effectivity of the individual subparts, we investigate variants of our approach with and without the spatial and/or the appearance prior.

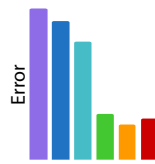
The classic baselines are MEAN and BILATERAL [6] filters, which are also unsupervised. We choose their parameters so that they are optimal on the training set in terms of our metric.

As supervised learning-based denoisers, we use the same architecture, as we have employed for the unsupervised setting, whereby we use the training algorithm proposed in PointCleanNet [21]. While this means, that we do not use the original PointCleanNet network architecture, which is based on PointNet, we believe that our evaluation is more insightful with a unified architecture – especially since the architecture employed by us has outperformed PointNet on a range of other tasks [13].

Finally, we study three variants of our approach. The first one is with NO PRIOR. The second we denote as NO COLOR, which is our prior but only based on proximity. The last one is FULL which includes all our contributions. More precisely, we use XYZ point clouds for NO PRIOR and NO COLOR and XYZRGB point clouds for FULL. Again, color is only used to sample the prior, not as an input to the network during training or testing.

Table 1. Error (less is better) per method on SIMPLE noise.

Ours					
Mean	Bilat.	No p.	No c.	Full	Sup.
.598	.592	.582	.547	.542	.545



Bar chart showing Error for different methods. The methods are Mean (violet), Bilat. (blue), No p. (cyan), No c. (green), Full (orange), and Sup. (red). The error values are: Mean (.598), Bilat. (.592), No p. (.582), No c. (.547), Full (.542), and Sup. (.545). The Full method has the lowest error.

5.2. Quantitative Results

Denoising performance. We start with SIMPLE noise and look into ADVANCED later. A comparison of the average error across the test set for different methods is shown in Tbl. 1, whereby each column represents one method. All methods are trained with the same amount of training exemplars, that is, 22 million points.

As can be seen, our full method (orange) performs best. We even outperform the supervised competitor (red), likely because the network has to find more valid generalizations and is less prone to over-fitting. As can also be seen, the other non-learned methods like mean (violet) and bilateral (blue) are not competitive, even when tuned to be optimal on training data. We further see a clear distinction between ablations of our method and the full approach. When training without a spatial prior (cyan), the method is much worse than supervised and only slightly better than mean. A method not using color for training (green) – but including the spatial prior – can achieve almost full performance, but only adding color will outperform supervised.

This comparison is on the same amount of data. However, in most real-world scenarios, the number of noisy point clouds can be assumed to be much higher than the amount of clean ones. We will study this relation next.

Supervision scalability. We will next simulate, how different methods scale with the amount of training data available. This is the number of clean point clouds for supervised, and the number of noisy point clouds for our method in all its variants.

The outcome is seen in Tbl. 2 where different methods are columns and different amounts of training data are rows. The plot to the right shows the relation as a graph. We show the logarithmic fit to the individual measurements shown as points. The color encoding is identical for all plots. The dif-

Table 2. Error (less is better) for different amount of supervision.

Train data	Ours			
	No p.	No c.	Full	Sup.
.5 M	.587	.557	.558	.574
1 M	.584	.550	.557	.563
4 M	.584	.553	.543	.546
22 M	.582	.547	.542	.545

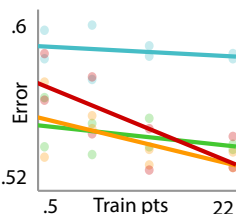
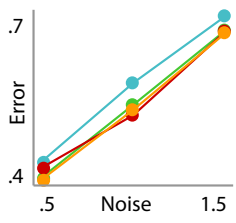


Table 3. Error (less is better) for different levels of SIMPLE noise.

Noise Levels	Ours			
	No p.	No c.	Full	Sup.
1.5 %	.734	.698	.691	.695
1.0 %	.578	.534	.525	.515
0.5 %	.435	.411	.408	.426



ference between the methods is measured wrt. the number of total training points ranging from .5 to 22 millions.

Not unexpected, we see all methods benefit from more training data. We see that our method performs better than supervised across a range of training data magnitudes. At around 22 million points, the highest we could measure, the red and orange lines of our full model and supervised cross. That only means, that after this point, our unsupervised method needs more training data to achieve the same performance as a supervised method.

We further see that the ablations of our method without a prior and without color do not only perform worse, but also scale less favorable, while ours (orange) is similar to supervised (red). Admittedly, supervised scales best.

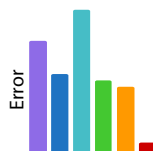
Amount of noise. While we have studied the average over three levels of noise in the previous plots, Tbl. 3 looks into the scalability with noise levels in units of scene diameter percentages. We find that error is increasing as expected with noise, but all methods do so in a similar fashion. In two cases, we win over supervised, in one case supervised wins, resulting in the improved average reported above.

Denoising performance. While we have studied SIMPLE Gaussian noise, we now relax this assumption and explore ADVANCED simulated scanner noise generated as explained in Sec. 5.1. While it is simulated, it has the benefit that the ground truth is known, which will not be the case for our experiments on real scanned data.

Tbl. 4 shows the error of different methods for this type of noise. We see, that in this case, our full method (orange) performs better than any other unsupervised method, such as mean or bilateral (violet and blue). A supervised method can perform better than other methods for this noise at the same amount of training data input, 12 million points. Finally, we also see that ablations without the suggested prior

Table 4. Error (less is better) per method on ADVANCED noise.

	Ours					
Mean	Bilat.	No p.	No c.	Full	Sup.	Error
.378	.362	.393	.359	.356	.329	



Method	Error
Mean	.378
Bilat.	.362
No p.	.393
No c.	.359
Full	.356
Sup.	.329

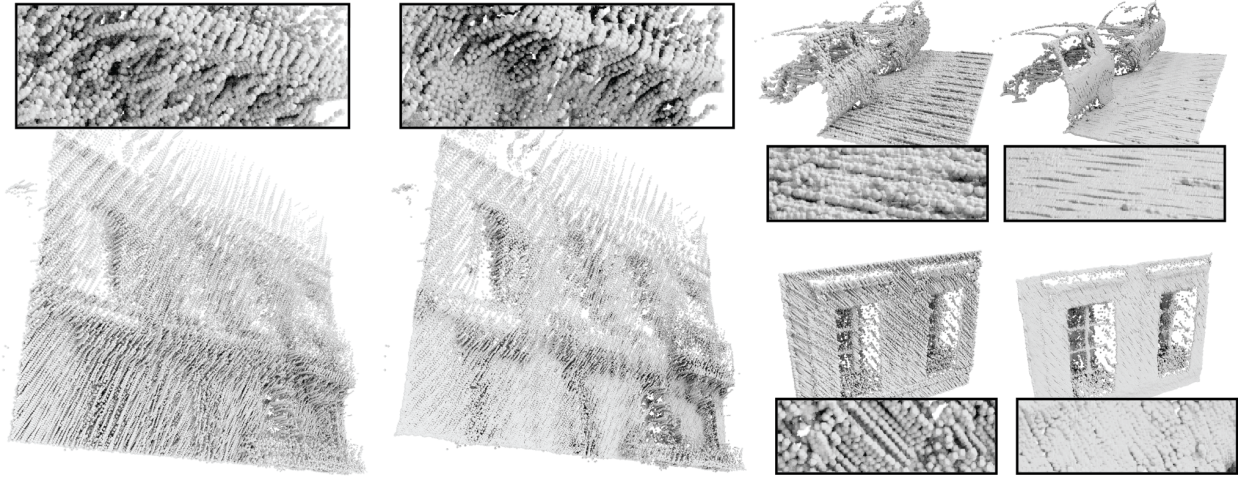


Figure 7. Multiple real world pairs of noisy input scans (*left*) and the result of our denoiser (*right*), accompanied by zoomed insets.

(cyan and green) have a higher error, indicating the priors are equally relevant for this type of noise, too.

5.3. Qualitative Results

Here, we repeat the above experiments, on real world noisy point clouds from a Mobile Laser Scanning setup based on a Velodyne HDL32 3D scanner. We used the Paris-rue-Madame data set [24] which is composed of 20 million points. We subdivide the model into parts of ca. 150 K points each, resulting in 17 million points used during training and 3 million points for testing. Note that in this setting, noise is part of the data and does not need to be simulated. Furthermore, and most important, no clean ground truth is available. Consequentially, the error cannot be quantified and we need to rely on human judgment.

We see in Fig. 7, how our method removes the noise and produces a clean point cloud without shrinking, with uniform sampling as well as details. We cannot apply a visualization of the error, as the ground truth is unknown. We instead provided point cloud renderings by representing the point clouds as a mesh of spheres with shading.

5.4. Ablation

No prior When not using the prior in space (green), the denoiser learned across different types of noise (Tbl. 1), magnitudes of noise (Tbl. 3) and amounts of training data (Tbl. 2) is consistently worse and not much better than Gaussian or bilateral. This indicates it is an essential contribution.

No appearance Making use of appearance consistently improves the outcome across the aforementioned three axes

of variations in Tbl. 1 (and Tbl. 4), Tbl. 2 and Tbl. 3, either taking the quality beyond supervision or very close to it, given the same data.

Varying prior shapes. Other compactly-supported smooth kernels popular in general MLS or point cloud denoising could be used instead of our Gaussians for k . We experimented with Gaussians at different α , Wendland [28] as well as inverse multi-quadratic, but found our choice to work best, as documented in the supplemental materials.

6. Conclusions

We have presented an unsupervised learning method to denoise 3D point clouds without needing access to clean examples, and not even noisy pairs. This allows the method to scale with natural data instead of clean CAD models decorated with synthetic noise. Our achievements were enabled by a network that maps the point cloud to itself in combination with a spatial locality and a bilateral appearance prior. Using appearance in the prior is optional, but can improve the result substantially, without even being input to the network, neither at test nor at training time. Denoising with color as input, as well as joint denoising of color and position, remains future work. Our results indicate we can outperform supervised methods, even with the same number of training examples.

Generalizations to other unstructured or semi-structured domains like animated point clouds or unstructured light fields provide a promising avenue of future research.

Acknowledgements This work was partially funded by the Deutsche Forschungsgemeinschaft (DFG) under grant RO 3408/2-1 (ProLint), the Federal Minister for Economic Affairs and Energy (BMWi) under grant ZF4483101ED7 (VR-Reconstruct), and a Google Faculty Research Award. We would like to acknowledge NVidia’s GPU donation for our training cluster.

References

- [1] M. Alexa, J. Behr, D. Cohen-Or, S. Fleishman, D. Levin, and C. T. Silva. Point set surfaces. In *Proc. VIS*, pages 21–28, 2001. 2
- [2] H. Avron, A. Sharf, C. Greif, and D. Cohen-Or. l_1 -sparse reconstruction of sharp point set surfaces. *ACM Trans. Graph.*, 29(5):135, 2010. 2
- [3] J. Batson and L. Royer. Noise2Self: Blind denoising by self-supervision. *CoRR*, abs/1901.11365, 2019. 1, 2, 3
- [4] A. Buades, B. Coll, and J.-M. Morel. A non-local algorithm for image denoising. In *CVPR*, volume 2, pages 60–5, 2005. 2
- [5] H. C. Burger, C. J. Schuler, and S. Harmeling. Image denoising: Can plain neural networks compete with bm3d? In *CVPR*, pages 2392–2399, 2012. 2
- [6] J. Digne and C. de Franchis. The Bilateral Filter for Point Clouds. *Image Processing On Line*, 7:278–287, 2017. 2, 6
- [7] M. Elad and M. Aharon. Image denoising via sparse and redundant representations over learned dictionaries. *Trans. Image Processing*, 15(12):3736–45, 2006. 2
- [8] H. Fan, H. Su, and L. J. Guibas. A point set generation network for 3d object reconstruction from a single image. *CoRR*, abs/1612.00603, 2016. 6
- [9] S. Fleishman, I. Drori, and D. Cohen-Or. Bilateral mesh denoising. In *ACM Trans. Graph.*, volume 22, pages 950–3, 2003. 2
- [10] G. H. Golub and C. F. Van Loan. An analysis of the total least squares problem. *SIAM J Numerical Analysis*, 17(6):883–893, 1980. 1
- [11] M. Gschwandtner, R. Kwitt, A. Uhl, and W. Pree. Blensor: blender sensor simulation toolbox. In *International Symposium on Visual Computing*, pages 199–208. Springer, 2011. 6
- [12] P. Guerrero, Y. Kleiman, M. Ovsjanikov, and N. J. Mitra. PCPNET: learning local shape properties from raw point clouds. *CoRR*, abs/1710.04954, 2017. 2
- [13] P. Hermosilla, T. Ritschel, P.-P. Vazquez, A. Vinacua, and T. Ropinski. Monte Carlo convolution for learning on non-uniformly sampled point clouds. *ACM Trans. Graph.*, 37(6), 2018. 3, 5, 6
- [14] A. K. Jain. *Fundamentals of digital image processing*. Englewood Cliffs, NJ: Prentice Hall., 1989. 2
- [15] D. P. Kingma and J. Ba. Adam: A method for stochastic optimization. *CoRR*, abs/1412.6980, 2014. 5
- [16] A. Krull, T. Buchholz, and F. Jug. Noise2Void - learning denoising from single noisy images. *CoRR*, abs/1811.10980, 2018. 1, 2, 3
- [17] I.-K. Lee. Curve reconstruction from unorganized points. *Computer aided geometric design*, 17(2):161–177, 2000. 2
- [18] J. Lehtinen, J. Munkberg, J. Hasselgren, S. Laine, T. Karras, M. Aittala, and T. Aila. Noise2Noise: Learning image restoration without clean data. 2018. 1, 2, 3, 5
- [19] M. Levoy and T. Whitted. *The use of points as a display primitive*. UNC Chapel Hill Technical Report, 1985. 2
- [20] C. R. Qi, H. Su, K. Mo, and L. J. Guibas. Pointnet: Deep learning on point sets for 3d classification and segmentation. *CoRR*, abs/1612.00593, 2016. 1, 2, 3
- [21] M. Rakotosaona, V. L. Barbera, P. Guerrero, N. J. Mitra, and M. Ovsjanikov. POINTCLEANET: learning to denoise and remove outliers from dense point clouds. 2019. 2, 3, 5, 6
- [22] G. Rosman, A. Dubrovina, and R. Kimmel. Patch-collaborative spectral point-cloud denoising. In *Computer Graphics Forum*, volume 32, pages 1–12, 2013. 2
- [23] R. Roveri, A. C. Öztireli, I. Pandele, and M. H. Gross. Pointprons: Consolidation of point clouds with convolutional neural networks. *Comput. Graph. Forum*, 37(2):87–99, 2018. 2, 3
- [24] A. Serna, B. Marcotegui, F. Goulette, and J.-E. Deschaud. Paris-rue-madame database - a 3d mobile laser scanner dataset for benchmarking urban detection, segmentation and classification methods. In *ICPRAM*, 2014. 8
- [25] C. Tomasi and R. Manduchi. Bilateral filtering for gray and color images. In *ICCV*, page 839, 1998. 2
- [26] P. Vincent, H. Larochelle, I. Lajoie, Y. Bengio, and P.-A. Manzagol. Stacked denoising autoencoders: Learning useful representations in a deep network with a local denoising criterion. *J Machine Learning Research*, 11:3371–408, 2010. 2
- [27] L.-Y. Wei. Parallel poisson disk sampling. *ACM Trans. Graph.*, 27(3):20:1–20:9, 2008. 6
- [28] H. Wendland. Piecewise polynomial, positive definite and compactly supported radial functions of minimal degree. *Advances in computational Mathematics*, 4(1):389–96, 1995. 8
- [29] Z. Wu, S. Song, A. Khosla, F. Yu, L. Zhang, X. Tang, and J. Xiao. 3d shapenets: A deep representation for volumetric shapes. In *CVPR*, pages 1912–1920, June 2015. 6

Supplementary material

A. Error distribution

We studied the distribution of points wrt. the distance to the underlying surface in our test dataset. Fig. 8 (left) presents a histogram with the results of such study. Here we can see how the distribution of points has its maximum at distance 0.0 from the real surface and decreases with distance, following the same distribution as in the supervised setting.

B. Convergence

Fig. 8 (right) illustrates the evaluation error during training for two networks trained on the smallest dataset (.5 Million points). One network is trained with our algorithm (FULL) and the other one with supervised training. We can see that in both cases the loss decreases during training similarly. However, our algorithm converges to a lower error than supervised learning. With more training data, this gap is reduced until the curves cross.

C. Prior Kernel

We experimented with different kernels for our prior: Gaussian (k_g), Wendland (k_w), and Inverse Multi-Quadric (k_i). All kernels were adjusted to fit in the range $[-1, 1]$:

$$k_g(\mathbf{d}) = \frac{1}{\sigma\sqrt{2\pi}} \exp\left(-\frac{\|\mathbf{W}\mathbf{d}\|_2^2}{2\sigma^2}\right),$$

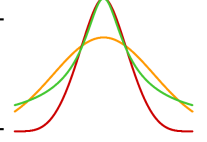
$$k_w(\mathbf{d}) = (1 - \|\mathbf{W}\mathbf{d}\|_2^2)^4 (1 + 4\|\mathbf{W}\mathbf{d}\|_2^2),$$

$$k_i(\mathbf{d}) = \frac{1}{\sqrt{1 + (5\|\mathbf{W}\mathbf{d}\|_2^2)^2}},$$

where $\mathbf{W} = \text{diag}(w)$ and $w = 1/\alpha r$. We performed an ablation study for different values of α and for each kernel

Table 5. Error obtained for different functions used as our prior.

Prior	α_1	α_2	α_3
Gauss. (k_g) ●	.567	.548	.556
Wedland (k_w) ●	.595	.560	.561
Inv. MQ (k_i) ●	.577	.577	.582



independently. For the Gaussian kernel we used $\alpha_1 = .3$, $\alpha_2 = .5$, and $\alpha_3 = .7$, and for the Wendland and Inverse Multi-Quadric kernel we used $\alpha_1 = .8$, $\alpha_2 = 1.$, and $\alpha_3 = 1.2$. Table Tbl. 5 show that the best performance was obtained by the Gaussian kernel.

D. Additional Qualitative Results

Fig. 10 and Fig. 9 provide more qualitative results on all the datasets used in the evaluation. Fig. 10 presents a visual encoding of the distance of each point to the real surface after applying the different networks for the simulated datasets. We can see how our algorithm obtains a quality similar to the network trained with supervised data. Fig. 9 illustrates the result of applying our network (trained on a real dataset) to a scanned model composed of 800 K points.

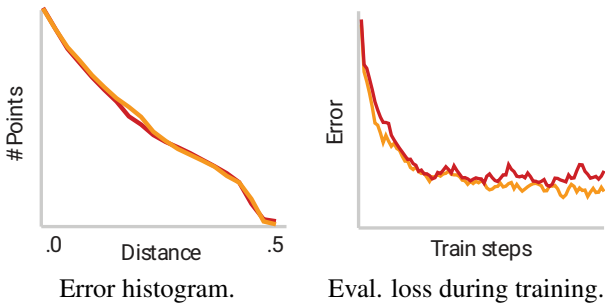


Figure 8. Ours (FULL) ● vs Supervised ●

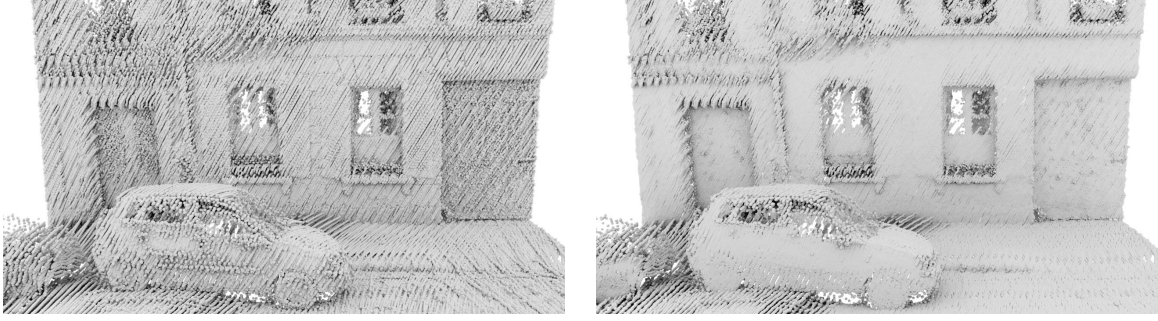


Figure 9. Comparison of our denoising algorithm (**right**) with the noisy scanned data (**left**) for a model composed of 800 K points.

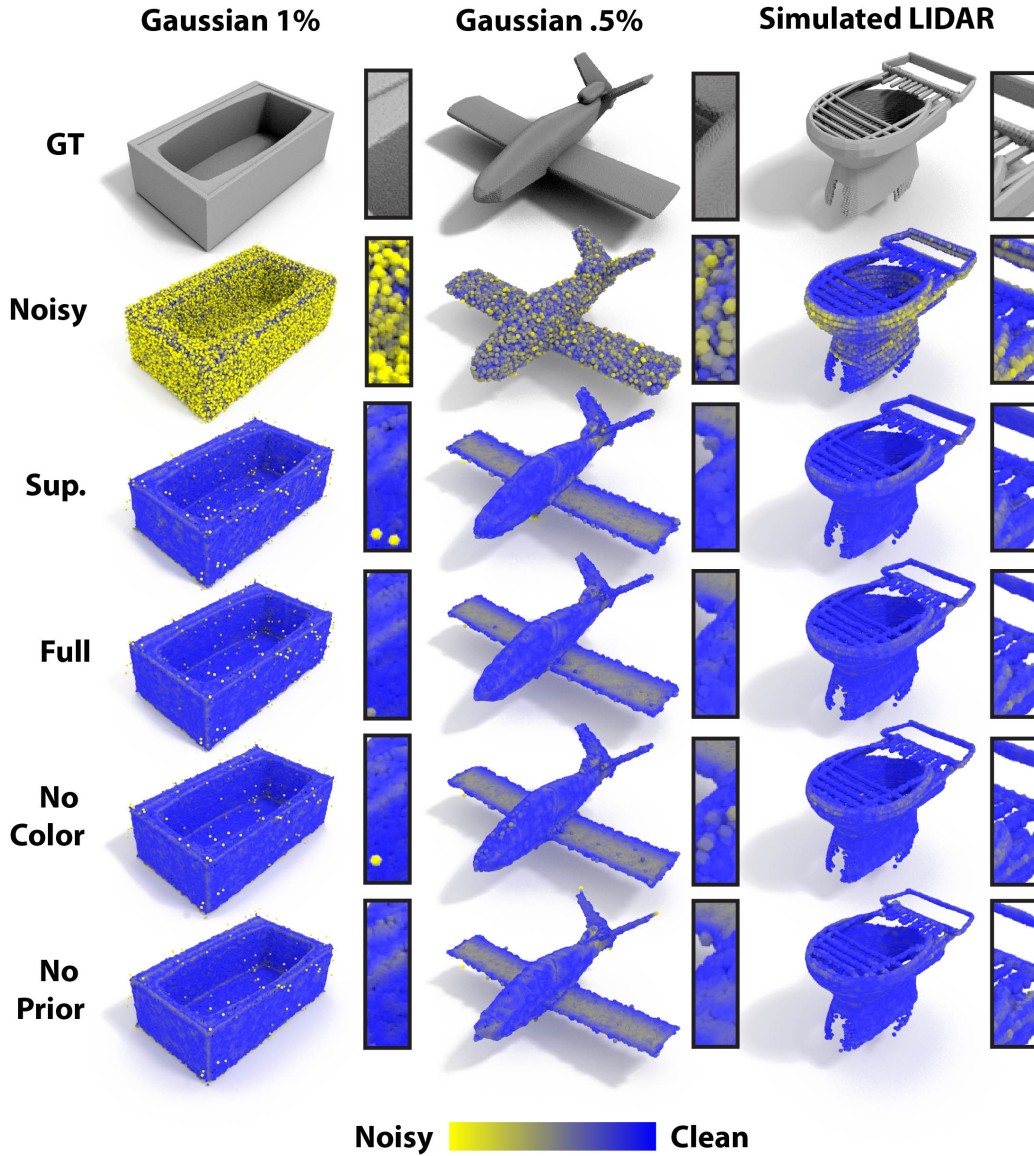


Figure 10. Visual encoding of the distance from each point to the underlying ground truth surface. Here blue indicates zero distance to the surface and yellow 2% of the diagonal of the model. We can see that for the two simulated datasets with different levels of noise, our algorithm achieves (**Full**) almost the same quality as a network trained with supervised data (**Sup.**). Moreover, we evaluated two variants of our training procedure: a prior without color information (**No Color**), and **No Prior**.